Numerical Simulation of High-Current Vacuum Arcs in External Magnetic Fields

E. Schade, D. Shmelev*

ABB Corporate Research, CH-5405 Baden/Switzerland
** Institute of Electrophysics RAS, 620016 Ekaterinburg, Russia, E-mail: shmelev@iep.uran.ru*

Abstract – High-current arcs as found in AMF vacuum interrupters have been numerically simulated taking into account the effect of evaporation of metal vapor from the anode surface. The physical behavior has been studied and the heat flux to the anode determined. Rise of surface temperature and rate of evaporation has been analyzed for arcing with one half wave of 50 Hz-AC-current between Cu contacts.

1. Introduction

The numerical simulations concentrate on high-current vacuum arcs, as e.g. arcs of vacuum interrupters at current interruption limit. The present study is a continuation of [1]. But now, the effects of essential evaporation from the anode are taken into consideration. The intense energy flux from the arc raises anode surface temperature. During arcing melting temperature will be exceeded soon, a pool of liquid forms at the anode surface, and maybe boiling temperature is approached finally. High density of metal vapor limits the interruption capability [2, 3]. Therefore, prediction of metal vapor production at contact surfaces as well as determination of contact erosion is of great importance in connection with the development of vacuum interrupters.

The arcing arrangement consists of two Cu contacts with 55 mm diameter, and fix contact distance of 10 mm as in [1]. The area effectively covered with cathode spots is reduced to 75% of contact area in order to consider the effect of shrinking of cathode connection diameter with increasing arc current.

2. Physical Model

Plasma behavior and heat flux to the anode are simulated for steady state conditions, i.e. constant arc current. It approximates well arcing with 50 Hz-AC-currents as for vacuum interrupter, because arc current changes much slower than relaxation is able to follow. Rotational symmetry is assumed (Fig. 1). The dashed line indicates the domain of computation. The externally applied axial magnetic field of strength B_{AMF} is homogeneously distributed in the area between the contacts. The arc plasma flows from cathode to anode under the action of forces of pressure together with (jxB)-forces. The plasma material originates from the cathode spots hosted at the cathode surface and, when anode surface temperature is high enough, from evaporation of metal vapor from anode surface. The cathode spots are to be evenly distributed within the effective part of cathode. The vapor from anode is ionized by electron impact. The flow of plasma from cathode enters the domain of calculation mixed up homogenously and with only an axial flow component. The mixing of plasma occurs within a mixing zone of short depth. The vapor at anode enters the plasma in axial direction with thermal velocity corresponding to surface temperature.

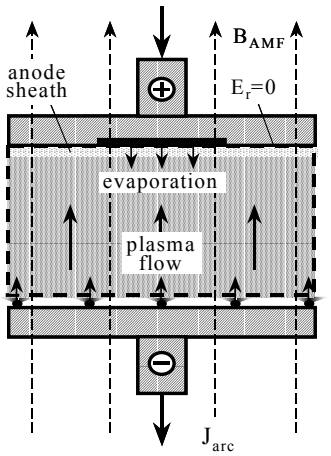

Fig. 1. Sketch of the model

The plasma consists of interpenetrating fluids of differently charged ions, electrons and neutrals with temperatures T_i, T_e and T_0, and velocities u, v and u_0, respectively.

Radial spread of arc plasma is hindered by (jxB)-forces resulting from self-magnetic field and externally applied B_{AMF}. Anode is a perfect sink for material fluxes contacting it.

The dissipated energy, the product of arc current J_{arc} multiplied by the potential difference between contacts, U_{arc}, is dominantly released to the contact. The residual part is carried away by radial outflow of plasma, and through emission of radiation from the plasma (radiation cooling).

The energy flux to anode results from the deposition of kinetic energy, ionization and condensation energy as well as work function of the ions and electrons arriving at anode. Absorption of radiation will be a minor contribution.

3. Set of Equations

The conditions of plasma allow the application of the single-fluid Magneto-Hydro-Dynamic (MHD) approach [4], based on the continuity equations of mass, momentum and energy, in combination with Maxwell's equations. It is described in detail elsewhere [1]. Here, only those equations are given, which had to be adapted to include the effect of metal vapor evaporation from the anode. These are equations (1) to (5). Equations (1) are the mass balances for neutral vapor n_0 and ions n_i considering ionization of vapor and recombination of ions with electrons. Equations (2) and (3) are the momentum balances for ions, and for neutrals, considering the gain and loss of momentum due to ionization. Equations (4) and (5) are the energy balances for ions and electrons respectively. The neutral vapor is assumed to have anode surface temperature. The energy exchange between ions and vapor atoms is slow and the live time vapor before ionization is short. Then electrons ionize quickly the vapor within a short distance from anode, as can be deduced from Fig. 6.

$$\frac{\partial n_0}{\partial t} + \operatorname{div} n_0 \vec{u} \;= -\dot{n} \quad \frac{\partial n_i}{\partial t} + \operatorname{div} n_i \vec{u} = \dot{n}; \qquad (1)$$

$$m n_i \left(\frac{\partial \vec{u}}{\partial t} + \vec{u} \cdot \vec{\nabla} \vec{u} \right) = \dot{n} \cdot \vec{u}_0 - \vec{\nabla} \left(n_e T_e + n_i T_i \right) + \frac{1}{c} \left[\vec{J} \times \vec{B} \right]; \qquad (2)$$

$$m n_0 \left(\frac{\partial \vec{u}_0}{\partial t} + \vec{u}_0 \cdot \vec{\nabla} \vec{u}_0 \right) = -\dot{n} \cdot \vec{u}_0 - \vec{\nabla} n_0 T_0; \qquad (3)$$

$$\frac{3}{2} n_i \left(\frac{\partial T_i}{\partial t} + u \cdot \vec{\nabla} T_i \right) + n_i T_i \operatorname{div} \vec{u} = \\ = \frac{3}{2} \dot{n} \cdot T_0 + \frac{3 m_e}{m} \frac{n_e}{\tau_{ei}} \left(T_e - T_i \right); \qquad (4)$$

$$\frac{3}{2} n_e \left(\frac{\partial T_e}{\partial t} + \vec{v} \cdot \vec{\nabla} T_e \right) + n_e T_e \operatorname{div} \vec{v} + \operatorname{div} \vec{Q}_e = \\ = -7.72 \cdot \dot{n} - 3 \frac{m_e}{m} \frac{n_e}{\tau_{ei}} \left(T_e - T_i \right) + \frac{\vec{J}^2}{\sigma} + \frac{\beta}{e} \vec{J} \cdot \vec{\nabla} T_e - R. \qquad (5)$$

The heat flux from plasma to anode rises the surface temperature of anode. Melting temperature (Fig. 3) is exceeded at about 22 kA in present case (Fig. 10), and finally boiling temperature is approached at high arc currents ([1, 5]). The numerical solution of time-dependent heat equation for the liquid pool and adjacent solid material delivers the surface temperature T_{surf} in dependence of heat flux, as described in [5], assuming arcing with one half wave of 50Hz-AC-current (Fig. 2). The heat flux density q_{anode} as function of current is taken from Fig. 11. The set of equations (6) describes anode evaporation. Here $g_{0,anode}$ is the flux density of evaporated material leaving the anode surface with average thermal velocity corresponding to T_{surf}; p_{equi} is the vapor pressure under equilibrium conditions; $g_{0,back}$ is the flow of metal atoms from the vapor cloud in front of anode back to anode. The difference between $g_{0,anode}$ and $g_{0,back}$ is the net flux of metal atoms g_{net}, entering the arc plasma. g_{dep} is the flux of deposition of material, whereas g_i is the flux of ions arriving at anode.

$$g_{0,anode} = p_{equi} (2\pi m T_{surf})^{-1/2}, \\ g_{0,back} = p_0 (2\pi m T_0)^{-1/2}, \qquad (6)$$

$$g_{net} = g_{0,anode} - g_{0,back} = g_{0,anode} \left(1 - \frac{p_0}{p_{equi}} \right), \\ g_{dep} = g_{net} - g_i, \; g_i = n_i u_z, \; g_{0,anode} = u_0 n_{vap}.$$

4. Obtained results

Figures 4 and 5 exhibit the behavior of evaporation. When boiling temperature is approached, strong evaporation cooling diminishes the energy input into the contact. Consequently further increase of surface temperature as well as rate of net evaporation slows down as e.g. demonstrated by Fig. 3 at 50 kA for the surface temperature T_{surf} and Fig. 4 for the net flux of evaporated metal atoms g_{net} respectively.

Figure 5 compares the total particle net flux from anode $g_{anode,net}$ (a) with the total particle flux from cathode and (b) with the total particle flux released into plasma from the both material sources, i.e. cathode and anode, in dependence of arc current. The total particle flux into plasma is composed of the ion flux from cathode and the net flux of evaporated material g_{net}. The latter flux returns to anode as ionized material. Whereas proportion (a) of Fig. 5 increases steadily with current and exceeds 100% easily, the proportion (b) levels off at about 75% at high currents.

The slower ions resulting from vapor ionization are quickly integrated into the background plasma due to strong ion-ion interaction. They pick up the temperature of the ions coming from cathode as well as the high anode-directed velocity of cathode ions. The evaporated anode material is brought back to anode and hindered to reach the cathode.

Figures 7 and 8 demonstrate the resulting increase of ion density in front of anode. The pressure in front of the anode increases with current also, but it is still lower than at cathode side (Fig. 9). Fig. 7 exhibits the constriction of plasma, which is followed by expansion closer to anode due to the effect of evaporation from anode at high currents. It reflexes the typical features of appearance of the diffuse columnar arc mode as described by [6] and [1]. It supports the suggestion, the transition from diffuse arc mode to diffuse columnar arc mode as well as the behavior of latter is caused by the additional release of material from anode, i.e. contact evaporation, as assumed in [1].

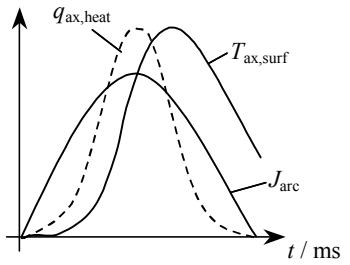

Fig. 2. Arcing with one half-wave of 50 Hz-AC-curretnt J_{arc}

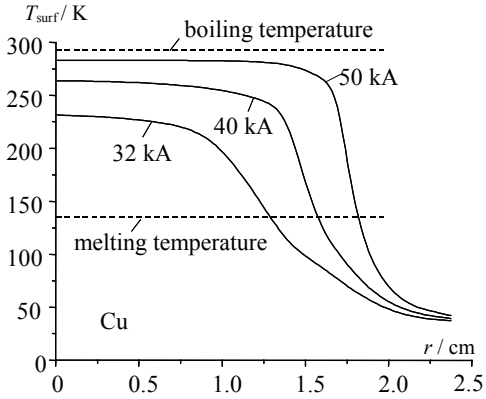

Fig. 3. Radial distribution of anode surface temperature for different arc currents

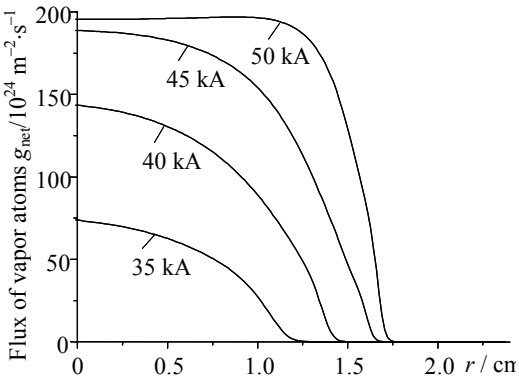

Fig. 4. Radial distribution of flux of vapor atoms evaporated from anode gnet for different arc currents

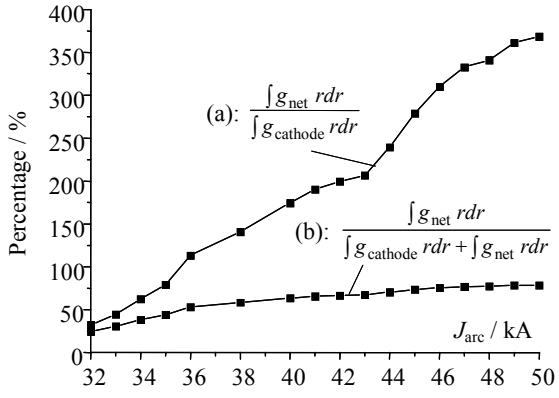

Fig. 5. Net vapor flux released into plasma (a) relative to ion flux from cathode only and (b) relative to total particle flux released into plasma respectively

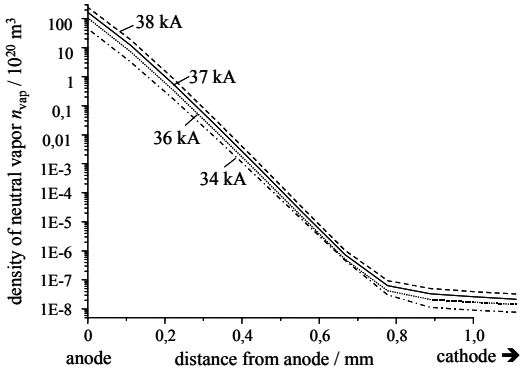

Fig. 6. Density of metal vapor, i.e. Cu atoms, along axis from anode to cathode for different arc currents

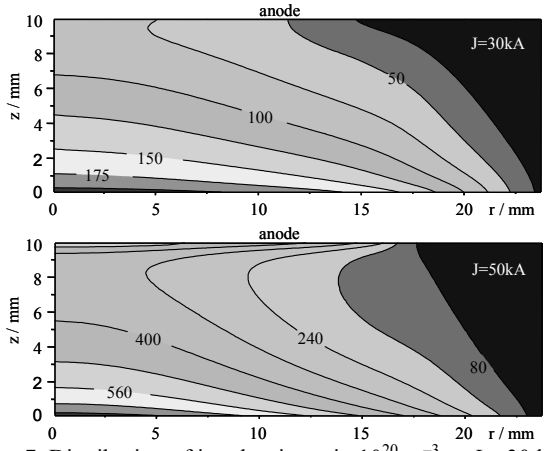

Fig. 7. Distribution of ion density n_i in 10^{20} m^{-3} at J = 30 kA (above) and 50 kA (below)

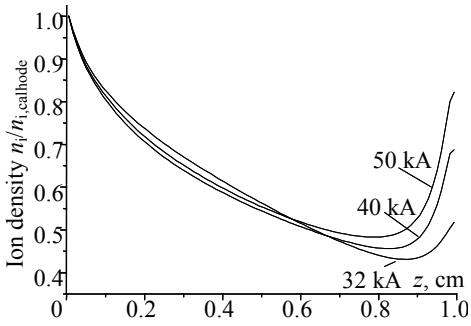

Fig. 8. Distribution of ion density n_i along center axis from cathode to anode for different arc currents, normalized to ion density at cathode

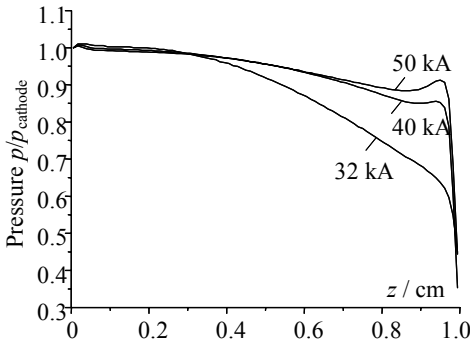

Fig. 9. Distribution of pressure along center axis from cathode to anode for different arc currents, normalized to pressure at cathode

Figure 10 shows the radial distributions of density of electron current $j_{electron}$, of ion current j_{ion} and of current density j at J_{arc} = 50 kA, together with the radial distribution of heat flux to anode q_{anode}. The current density is highest outside of center. It is caused by the strong evaporation from anode. The current density of electrons $j_{electron}$ is higher than the current density j, because it has compensated the high ion current density j_{ion}. Ion current flow is more than twice of total current.

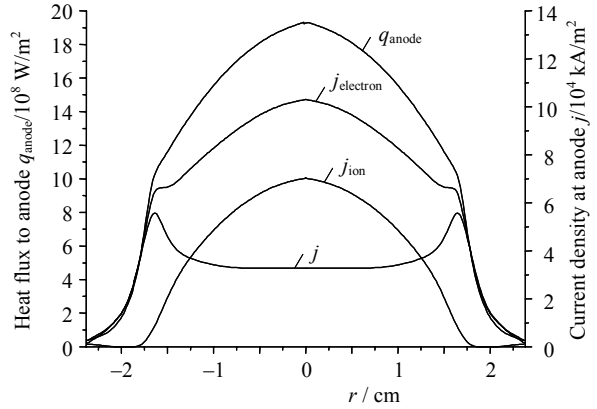

Fig. 10. Radial distribution of heat flux q_{anode}, and of density of electron current $j_{electron}$, of ion current j_{ion} and of total current j at J_{arc} = 50 kA

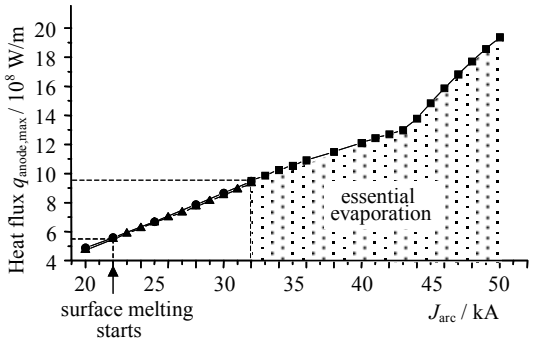

Fig. 11. Heat flux density at anode $q_{anode,max}$ as function of arc current J_{arc}

Fig. 10 shows an example of the radial distribution of the heat flux q_{anode} for 50 kA. Fig. 11 depicts the maximal value of heat flux to anode $q_{anode,max}$ as function of arc current J_{arc}. Assuming arcing with one half wave of 50Hz-AC-current melting of anode surface starts at about J_{arc} = 22 kA, but relevant evaporation occurs only when the heat flux density q_{anode} approaches values of about 10^9 W/m^2, at about 32 kA in present case. The function of heat flux density from arc current depends on the arcing arrangement. The interrelation of the different physical processes is complex. Corresponding to Fig. 11, heat flux density increases with J_{arc} about linearly up to 35 kA, then, up to 43 kA, increase slows down a little bit because high plasma density at anode reduces constriction. Rate of increase of heat flux rises when surface temperature comes close to boiling temperature at 43 kA and net flux of evaporation reduces (Figs. 3, 4).

5. Discussion and Conclusions

Present numerical modeling has proved to provide essential input for the understanding of the complex interrelation of the different physical phenomena of high-current vacuum arcs with anode evaporation, and to be a valuable tool for research and development. The improvement of knowledge concerns the physical phenomena at current interruption limit of vacuum switches.

Contact evaporation has strong impact on arc behavior. With anode evaporation arc appearance adopts the typical features of diffuse columnar arcs as experimentally observed by [6].

Effects of melt at anode surface, as e.g. movement of liquid material, has been not yet considered. Further, the influence of cathode connection is only approximated. Constant reduction of cathode is assumed, independent of arc current. With rising arc currents, the effective area of cathode connection shrinks, and cathode evaporation of similar strength seems to take place, as can be deduced from the measurements of [6]. But heat flux to anode increases strongly with reduction of effective cathode area [1]. Future modeling has to incorporate the dynamical behavior of cathode connection, including heating of cathode surface, resulting evaporation and loss of plasma due to back flow to cathode.

Unfortunately experimental results are rare, but they are urgently needed for further improvement of the physical models as well as for validation of the numerical predictions.

References

[1] E. Schade and D. Shmelev, IEEE Trans. on Plasma Science **31**,890–901 (2003).

[2] R. Gilles, K.D. Weltmann, E. Schade, M. Claessens, IEEE Trans. on Plasma Science **29**, 754–758 (2001).

[3] E. Schade and E. Dullni, IEEE Trans. on Dielectrics and Electrical Insulation **9**, 207–215 (2002).

[4] S.I. Braginskii, *Transport Processes in a Plasma, in: Reviews of Plasma Physics,* M.A. Leontovich, Ed., Consultants Bureau, New York, 1965.

[5] E. Schade, D. Shmelev, and I. Kleberg, *in: Proc. 21st International Conference on Electrical Contacts (ICEC),* Zurich (Switzerland), 2002, 518–525.

[6] H. Schellekens and M.B. Schulman, IEEE Trans. Plasma Science **29**, 452–461 (2001).